Springer

KSME

Journal of Mechanical Science and Technology 31 (3) (2017) 1169~1179
www.springerlink.com/content/1738-494x(Print)/1976-3824(Online)
DOI 10.1007/s12206-017-0215-0

Investigation of strut-ramp injector in a Scramjet combustor: Effect of strut geometry, fuel and jet diameter on mixing characteristics †

Rahul Kumar Soni and Ashoke De*

Department of Aerospace Engineering, Indian Institute of Technology Kanpur, Kanpur 208016, India

(Manuscript Received April 27, 2016; Revised September 16, 2016; Accepted November 7, 2016)

Abstract

The strut-based injector has been found to be one of the most promising injector designs for a supersonic combustor, offering enhanced mixing of fuel and air. The mixing and flow field characteristics of the straight (SS) and Tapered strut (TS), with fixed ramp angle and height at freestream Mach number 2 in conjunction with fuel injection at Mach 2.3 have been investigated numerically and reported. In the present investigation, hydrogen (H_2) and ethylene (C_2H_4) are injected in oncoming supersonic flow from the back of the strut, where jet to freestream momentum ratio is maintained at 0.79 and 0.69 for H_2 and C_2H_4, respectively. The predicted wall static pressure and species mole fractions at various downstream locations are compared with the experimental data for TS case with 0.6 mm jet diameter and found to be in good agreement. Further, the effect of jet diameter and strut geometry on the near field mixing in strut ramp configuration is discussed for both the fuels. The numerical results are assessed based on various parameters for the performance evaluation of different strut ramp configurations. The SS configuration for both the injectant has been found to be an optimum candidate; also it is observed that for higher jet diameter larger combustor length is required to achieve satisfactory near field mixing.

Keywords: Ethylene; Hydrogen; Mixing; Strut-ramp; Total pressure decay

1. Introduction

The development of a high-speed propulsion system requires a thorough understanding of the complex flow physics associated with the combustor. Over the years, the research community has found Scramjet engines to be the most efficient air-breathing propulsion system in the high-speed flow regime. However, due to intrinsic difficulties associated with the combustion mechanism in a supersonic flow, there exists a need for development in the area of fuel mixing and flame holding. At higher supersonic speeds, the residence time for ingested air within the Scramjet unit is on the order of milliseconds; in turn, it means that the fuel injected in the oncoming air must mix efficiently and burn to release energy within few milliseconds. Hence, the very first step towards enhanced combustion efficiency could be attained by designing an efficient mixing strategy which can offer stable operating condition (or stabilized flame front). Various researchers over the year have explored a wide range of injection mechanisms that include splitter plate, normal injection, compression/expansion ramps, and lobe mixer; many more detailed reviews regarding the same can be found in Ref. [1].

The earlier injection strategy involved transverse injection onto the oncoming supersonic crossflow [2-8]. Transverse injections lead to the formation of normal bow shock separating two regions of flow: upstream and downstream. A recirculation zone is created at the downstream, which aids in flame holding and thereby offering higher combustion efficiency. The total pressure loss, however due to a normal shock wave is significantly high and affects the scramjet cycle performance. However, various studies [9-16] suggest that the strut based parallel injection is more promising, as it offers the possibility of injecting fuel into the core of oncoming supersonic flow, leading to uniform spreading of the fuel. The parallel injection system is also known to offer improved cycle performance, whereas the combustion efficiency is reduced due to deterioration in near field mixing. Diamotakis [10] reported that the mixing in a parallel injection system could be improvised with the generation of axial vorticity. This led to the research into the various strut designs. The presence of a strut leads to the bifurcation of oncoming supersonic flow, which enhances the mixing due to formation of the shear layer behind the strut. Another important phenomenon contributing towards the mixing enhancement is the shock-shear layer interaction. The shock generated at the ramp (wedge) leading edge undergoes reflection and continuously interacts with the supersonic shear layer leading to the generation of vorticity

*Corresponding author. Tel.: +91 5122597863, Fax.: +91 5122597561
E-mail address: ashoke@iitk.ac.in
† Recommended by Associate Editor Kyu Hong Kim

through the baroclinic torque mechanism [18-22]. Menon and Genin [12] in their study with injection through wedge observed that mixing in nonreacting cases is mainly due to unsteadiness and enhanced level of turbulence in the shear layer. This interaction perturbs the shear layer, the result of which is larger entrainment of surrounding air, which also contributes towards enhanced mixing.

Research on strut mixing devices covers a wide range of designs and includes both normal and parallel injection methodologies. Most struts consist of a ramp followed by the strut and fuel is injected from the strut. Dessornes and Jourdren [9] compared three mixing techniques for scramjet combustion: Transverse injection in a cavity, two-stage transverse injection and a strut consisting of a vertical wedge front with fuel injection at the back-side of the trailing edge. They found that a strut was the only technique that affected the entire flow field due to deeper penetration but had a higher pressure loss than the other techniques. The researchers suggest that more interest should be paid to the design of the strut to minimize the pressure loss while maintaining the ability to affect the flow field.

From the few existing studies, it has become evident that parallel injection into the core of oncoming supersonic flow is promising. However, there is still a need for extensive study to understand the flow physics and mixing characteristics for several possible configurations. Various parameters need to be investigated, such as ramp angle, strut length and lip thickness, which directly not only affects the mixing but also the length of the combustor required to achieve satisfactory mixing. To the best of authors' knowledge of the open literature, this type of investigation has not been reported, especially involving this particular configuration, whereas most studies in the past have focused mainly on lobed struts or cantilevered type injector. Only a study involving lip thickness variation as parameter for tapered strut with fixed diameter has been reported by Lee [20]. This paves the way for the current investigation with multiple parameters with emphasis on strut geometry as well. Hence, the primary motivation of the present work is to characterize the mean flow features to understand the mixing behaviour. Therefore, the present study is performed with two equation RANS (Reynolds averaged Navier Stokes) based model, as these models require lesser computational resource (cost effective) and offer good understanding of the mean flow field. In the present work, flow field and mixing characteristics for SS and TS injectors are investigated for hydrogen and ethylene. The effect of jet diameter (0.6, 1 and 2 mm) on flow features and mixing has been studied for both the fuels, including different strut configurations. In the case of SS configuration, only lip thickness varies due to jet diameter variation; however, in case of TS, both the taper angle and lip thickness vary to accommodate the given jet diameter. Initially, the validation and grid independence of the solver is demonstrated followed by the detailed parametric investigation on mixing characteristics.

2. Numerical details

2.1 Governing equations

The Favre-averaged governing equations for fluid motion are discretized and solved using the Finite-volume method (FVM). The equations for continuity, momentum, energy, species transport and turbulence transport are recast as:

Continuity:

$$\frac{\partial \overline{\rho}}{\partial t}+\frac{\partial \overline{\rho}\tilde{u}_i}{\partial x_i}=0\,. \tag{1}$$

Mometum:

$$\frac{\partial}{\partial t}\left(\overline{\rho}\tilde{u}_i\right)+\frac{\partial}{\partial x_j}[\overline{\rho}\tilde{u}_i\tilde{u}_j+\overline{p}\delta_{ij}+\overline{\rho u_i^{"}u_j^{"}}-\overline{\tau}_i]=0\,. \tag{2}$$

Energy:

$$\frac{\partial}{\partial t}\left(\overline{\rho}\tilde{E}\right)+\frac{\partial}{\partial x_j}[\overline{\rho}\tilde{u}_j\tilde{E}+\tilde{u}_j\overline{p}+\overline{u_j^{"}p}+\overline{\rho u_i^{"}E^{"}}+\overline{q_j}-\overline{u_i\tau_{ij}}]=0\,. \tag{3}$$

Species transport:

$$\frac{\partial}{\partial t}\left(\overline{\rho}\tilde{Y}_k\right)+\frac{\partial}{\partial x_j}\left(\overline{\rho}\tilde{u}_j\tilde{Y}_k\right)-\frac{\partial}{\partial x_j}\left(\overline{\rho D_k\frac{\partial Y_k}{\partial x_j}}-\overline{\rho u_i^{"}Y_k^{"}}\right)=0 \tag{4}$$

where (~) and (-) refer to density weighted time averaging and averaging through Reynolds decomposition, respectively. Y_k is the mass fraction of kth specie τ_{ij}, E and S_{ij} are shear stress, strain rate and total energy calculated as,

$$\overline{\tau_{ij}}=2\mu S_{ij}-\frac{2}{3}S_{kk}\delta_{ij} \tag{5}$$

$$S_{ij}=\frac{1}{2}\left(\frac{\partial u_i}{\partial x_j}+\frac{\partial u_j}{\partial x_i}\right) \tag{6}$$

$$\tilde{E}=e+\frac{\tilde{u}_k\tilde{u}_k}{2}+k \tag{7}$$

$$-\overline{\rho u_i^{"}u_j^{"}}=\mu_t\left(\frac{\partial u_i}{\partial x_j}+\frac{\partial u_j}{\partial x_i}\right)+\frac{2}{3}\rho k\delta_{ij}\,. \tag{8}$$

The μ_t in Eq. (8) is evaluated by complementing the above set of equations along with the transport equations of turbulence quantities. In the present study, the modified SST k-ω model proposed by Hellsten [23] is used to close the above set of equations. The eddy viscosity μt is given as,

$$\mu_t=\frac{\rho a_1 k}{max\left[a_1\omega,\Omega F_2\right]},\quad a_1=0.31 \tag{9}$$

$$F_2=tanh\left\{\left(max\left[2\frac{\sqrt{k}}{0.09\omega y},\frac{500\mu}{\rho y^2\omega}\right]\right)^2\right\} \tag{10}$$

$$\frac{\partial(\rho k)}{\partial t}+\frac{\partial}{\partial x_j}\left(\rho u_j k-\left(\mu+\sigma_k\mu_t\right)\frac{\partial k}{\partial x_j}\right)=\tau_{ij}\frac{\partial u_i}{\partial x_j}-\beta^*\rho\omega k \tag{11}$$

$$\frac{\partial(\rho\omega)}{\partial t}+\frac{\partial}{\partial x_j}\left(\rho u_j\,\omega-\left(\mu+\sigma_\omega\,\mu_t\right)\frac{\partial\omega}{\partial x_j}\right)=P_\omega-\beta\rho\omega^2$$

$$+2(1-F_1)\frac{\rho\sigma_{\omega2}}{\omega}\frac{\partial k}{\partial x_j}\frac{\partial\omega}{\partial x_j} \tag{12}$$

$$P_\omega=\frac{\gamma}{\nu_t}\tau_{ij}\frac{\partial u_i}{\partial x_j} \tag{13}$$

$$\tau_{ij}=\mu_t\left(2S_{ij}-\frac{2}{3}\frac{\partial u_k}{\partial x_k}\delta_{ij}\right)-\frac{2}{3}\rho k\delta_{ij} \tag{14}$$

$$\sigma_k=0.85,\quad \sigma_{\omega2}=0.856$$

$$F_1=tanh\left\{\left(min\left[max\left\{\frac{\sqrt{k}}{0.09\omega y},\frac{500\mu}{\rho y^2\omega}\right\},\frac{4\rho\sigma_{\omega2}k}{CD_{k\omega}\,y^2}\right]\right)^4\right\} \tag{15}$$

$$CD_{k\omega}=max\left[\frac{2\rho\sigma_{\omega2}}{\omega}\frac{\partial k}{\partial x_j}\frac{\partial\omega}{\partial x_j},\ 10^{-20}\right]. \tag{16}$$

Ω in Eq. (9) Ω is the vorticity magnitude and F2 is a blending function given by Eq. (10). The last term in Eq. (12) is cross diffusion term evaluated through Eq. (16) and production of ω is approximated through Eq. (13). Similar to F_2, F_1 is also a blending function given by Eq. (15). Further details about the Menter's model can be found in the Refs. [24, 25].

2.2 Numerical scheme

In the present work, the density based solver in OpenFOAM framework is modified to accommodate the transport of multi-species system, which is based on finite volume discretization utilizing semi-discrete, non-staggered central schemes for co-located variables on polyhedral mesh. The transport equations are solved using operator-splitting approach, where initially, convection of conserved variables is solved through explicit predictor equation and then diffusion of primitive variables is solved using implicit corrector equation. The solver utilizes central schemes proposed by Refs. [26, 27], which is an alternative approach to the Riemann solver offering accurate non-oscillatory solution. More detailed information about the implementation in OpenFOAM can be found in Ref. [28]. In present simulation, second-order backward Euler scheme is invoked for the time integration, whereas viscid and inviscid fluxes are discretized using central difference and TVD scheme. The parallel processing is achieved through the Message passing interface (MPI) technique.

2.3 Boundary details

At inlet, a fixed value is defined for all the variables as tabulated in Table 1. At the solid surface no-slip boundary condition is imposed, while at the outlet zero-gradient is used for all the variables excluding pressure for which a non-reflecting boundary condition is imposed to avoid the incoming waves to enter the domain. Note that the substantial difference in inlet velocity of hydrogen and ethylene (for same Mach number) is primarily due to the difference in specific heat ratio and gas constant. The Lewis number is assumed to be 1 in the present study. The simulation has been carried out for 30 non-dimensional times while maintaining CFL number below 0.5.

Table 1. Inlet conditions for main and jet flow.

Parameter	Air	Ethylene	Hydrogen
P_∞, Pa	49.5	29.5	29.5
T_∞, K	159	151	151
M_∞	2	2.3	2.3
U_∞, m/s	505	556	2203
Y_{N2}	0.76699	0	0
Y_{O2}	0.23301	0	0
Y_{C2H4}	0	1	0
Y_{H2}	0	0	1

Table 2. Grid spacing details.

	Jet region (mm)	Wall region (mm)
Grid 1	$\Delta x = 8\times10^{-03}$	$\Delta x = 5\times10^{-03}$
	$\Delta y = 6\times10^{-04}$	$\Delta y = 8\times10^{-04}$
Grid 2	$\Delta x = 5.1\times10^{-04}$	$\Delta x = 5.1\times10^{-04}$
	$\Delta y = 3\times10^{-05}$	$\Delta y = 1.4\times10^{-04}$
Grid 3	$\Delta x = 2.8\times10^{-05}$	$\Delta x = 2.8\times10^{-05}$
	$\Delta y = 1.4\times10^{-05}$	$\Delta y = 8.17\times10^{-05}$

The density based solver is modified to accommodate species transport equation and then validated against the experimental results of Gerlinger and Brüggemann [13]. The TS-0.6 mm configuration with H_2 as injectant is presented for solver validation and then detailed results for all the cases are discussed. The jet to freestream momentum ratio is 0.79 and 0.69, for the H_2 and C_2H_4 respectively. The ratio is defined as Jet momentum flux ratio = $(\gamma PM^2)_j/(\gamma PM^2)_\infty$.

3. Results and discussion

3.1 Grid independence and study

The grid is generated by creating multiple blocks to accommodate varying grid size using stretching function to maintain optimum grid size while resolving the important flow feature such as recirculation zone, shock, shock-shock interaction and shock-shear interaction. To perform the grid independence study, three sets of grids are generated: Grid1, Grid2 and Grid3 with 650×110, 1200×240 and 1950×450 cells, respectively.

The current flow involves a shock train throughout the channel length, which introduces a sharp gradient along both streamwise and transverse direction. The grid for the present computation is designed in such a manner that the near wall region is sufficiently resolved, and similarly the near jet region, between the two regions uniform stretching is utilized to keep the grid size optimum. Grid 1 has larger mesh gradient along

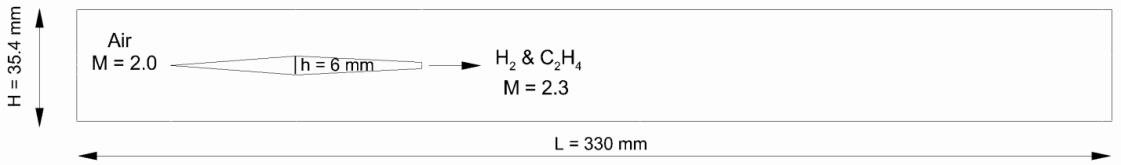

Fig. 1. Computation domain with dimension for TS -0.6 case.

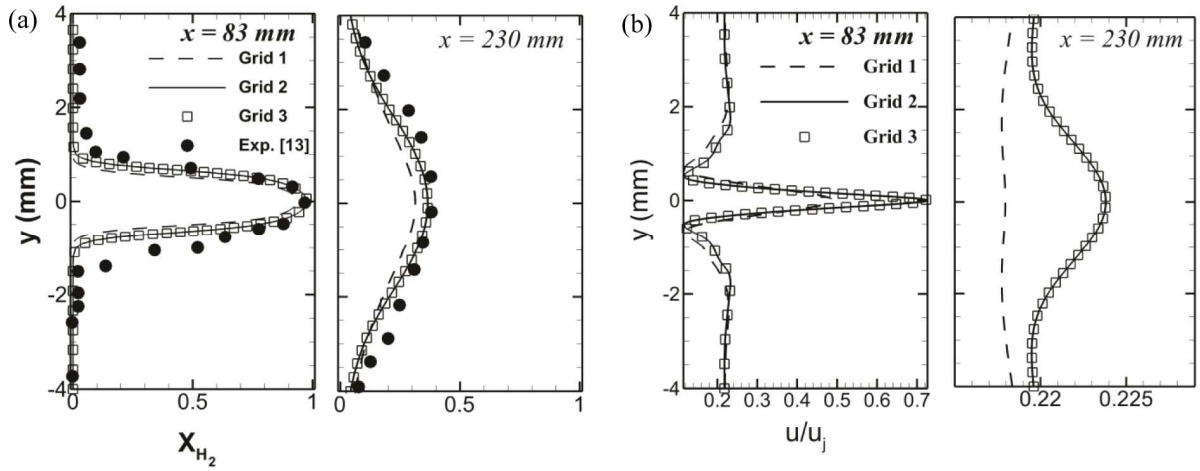

Fig. 2. (a) Mole fraction; (b) velocity profile for grid independence demonstration at two axial locations.

the transverse direction and this behavior can be attributed to the grid resolution along the transverse direction. Furthermore, the details of grid spacing are provided in Table 2 for better understanding.

The normalized velocity distribution for TS-0.6 mm case with hydrogen injection is presented in Fig. 2 to demonstrate the influence of the grid on numerical simulation. The experimental results are not available for the velocity; hence the quantitative comparison for the velocity field cannot be made. However, we have presented the quantitative comparison for H_2 mole fraction along with the velocity field for better assessment (Fig. 2).

It is quite evident from this figure that the results using both the grid 2 and grid 3 offer good agreement with the experimental data, which can be verified from the species mole fraction, and the discrepancies in grid 1 are primarily due to the improper predictions of velocity field.

The velocity distribution for grids 2 and 3 follows closely, but grid 1 shows under-prediction, especially at the downstream locations; in turn, this grid (Grid1) under-predicts the entrainment of the surrounding fluid. Also, qualitatively grid 1 under-predicts the recirculation zone present on the either side of the jet exit. The presence of the recirculation region compresses the jet, which then tends to spread out in cross-streamwise direction, downstream immediately. The predictions using grid 2 and grid 3 are in excellent agreement with each other; hence grid 2 is chosen for rest of the detailed computations and discussed hereafter.

The wall pressure distribution presented in Fig. 3 is compared to validate the solver alongside the observation of Ref. [13]. It is evident that both the numerical results follow closely and are in good agreement with the experimental data; however, there exists subtle differences as the former one [13] used different RANS models. Also, species mole fraction profiles of hydrogen and nitrogen are compared at four different locations which correspond to x = 83, 130 and 230 mm as depicted in Fig. 4.

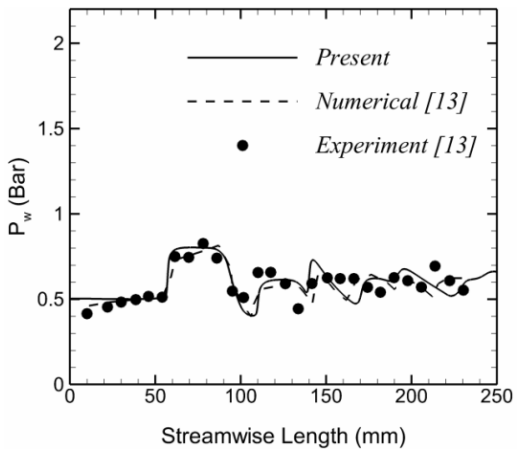

Fig. 3. Wall pressure distribution compared with numerical and experimental observation of Ref. [13].

As observed, at x = 83 mm, both nitrogen and hydrogen follow the experimental trend very nicely; however, as we move further downstream the jet diffusion in y-direction appears to

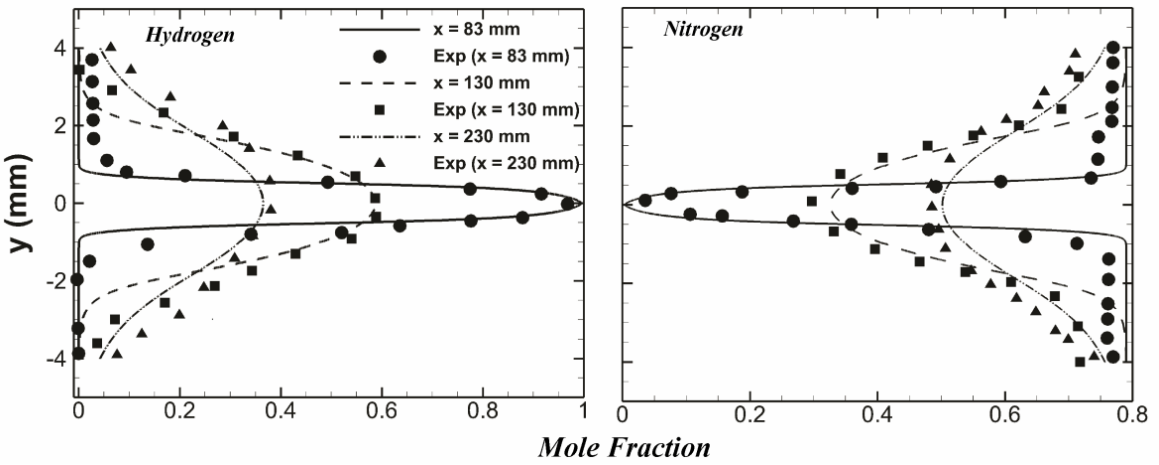

Fig. 4. Comparison of H_2 and N_2 mole fraction profile at various streamwise locations downstream of jet.

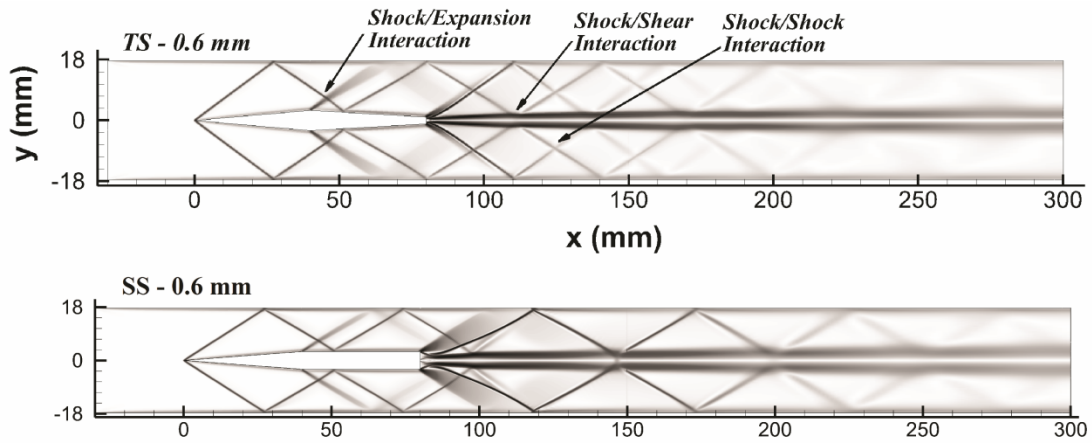

Fig. 5. Numerical Schlieren $(\nabla\rho)$ showing complex flow physics.

be slightly under-predicted but still yields reasonably accurate results. The difference along the wall normal direction can be attributed to the shift in shock locations, which is consistent with the observation of Ref. [13] and builds a scope for future investigation with high end turbulence models.

3.2 Flow features

The density gradient contour is presented in Fig. 5, where the complex flow features can be observed. Oblique shock wave is generated as the oncoming supersonic flow encounters the ramp, which is then reflected from the walls. Some of the main flow features observed are shock/shock, shock/boundary layer and shock/shear interaction. The reflected shock wave upon interacting with the shear layer produces vorticity, which leads to jet break up and aids in near field mixing. The flow on reaching the edge of strut reverses due to the finite lip thickness, which reattaches through the reattachment shock. This reattachment shock also contributes towards the vorticity production.

Another interesting phenomenon, which is evident from Fig. 5, is the interaction of shock wave and boundary layer along the channel wall. This interaction leads to the separation of boundary layer and vortical shedding past the separation point. In transverse injection where complicated shock structures (bow and lambda shock) are present, the separation of boundary layer due to shock formation introduces vortex shedding downstream of the jet injection.

These vortices transport the injectant and enhance the air/fuel mixing [29]. However, in the present case the shock/boundary layer interaction will have little or no effect on the mixing. Hence, the resolution of SWBLI is not of much relevance in the current computation.

The reattachment length and hence the reattachment shock strength varies depending on the lip thickness. The strength of recirculation also affects the mixing by altering the mixing layer thickness; larger recirculation zones are known to introduce higher level of turbulence. The extent of recirculation zone created at the strut corner has direct impact on the mixing and jet spreading, which will be discussed in the following section.

In Fig. 6, the close-up views of the jet for TS and SS configuration with 0.6 mm jet diameter are presented to get a qualitative estimate of the reattachment length. Evidently, a

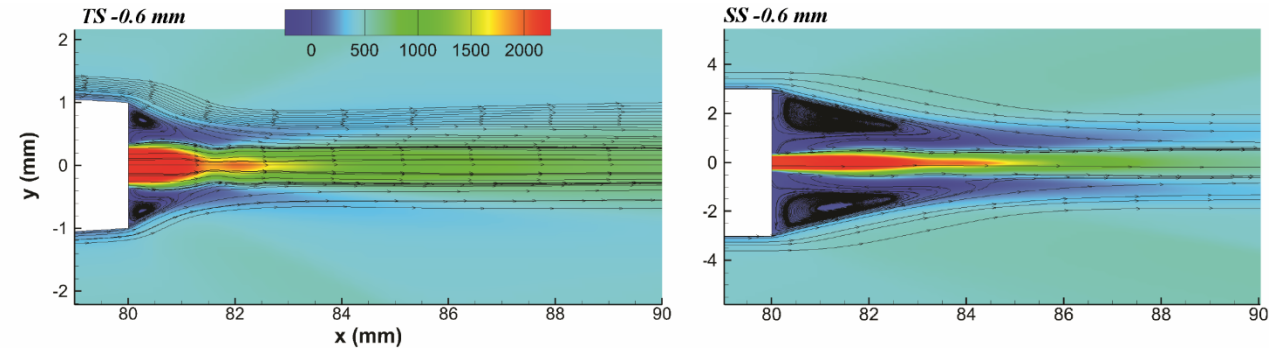

Fig. 6. Close-up view of 0.6 mm jet for both SS and TS configuration.3.3 effect of fuel and geometry.

huge difference can be observed in the size of the recirculation zone. For TS-0.6 mm case, the reattachment length is approximately 1.8 mm, but for SS-0.6 mm case much larger recirculation zone is observed, approximately 4.6 mm. At the point of reattachment, the jet core appears to be compressed due to the presence of the reattachment shock. This particular difference has considerable impact on the downstream flow features, as discussed in the following sub-sections.

For detailed parametric study, computations are performed for two different strut geometries, including three different jet diameters using two different fuels (H_2 and C_2H_4). For all cases reported in this section, the length and wedge angle are maintained constant. Fig. 7(a) shows the predicted hydrogen mole fraction at different stream-wise locations; where for a given jet diameter, the results of TS and SS cases are plotted for comparison. With the increasing jet diameter, the penetration in cross stream-wise direction enhances, i.e., jet spreading is more in radial direction; while a significant difference can be witnessed for the 0.6 mm and 1 mm cases for both TS and SS. However, with increasing jet diameter the performance along the stream-wise direction appears to deteriorate with the larger presence of hydrogen mole fraction. In case of 0.6 mm diameter, the difference between TS and SS configuration is more significant than 1 and 2 mm cases. The SS-0.6 mm case appears to have better performance in terms of near field mixing compared to TS-0.6 mm due to the significant difference in the extent of the recirculation region. In case of 1 and 2 mm cases for both the strut configurations, the difference is not very significant due to the presence of comparable recirculation zone. Overall, the stream-wise distribution for higher diameters for both the cases suggests that for higher jet diameter larger combustor length might be required to allow proper mixing. But this can be remedied by producing stronger shock, and hence the baroclinic torque, which will aid in early jet breakup and hence mixing augmentation.

Similarly, Fig. 7(a) presents the ethylene mole fraction distribution at different stream-wise locations for both the strut geometries. In contrast to H_2, ethylene seems to have better performance along the stream-wise direction but lesser diffusion in transverse direction.

The reason behind poor jet spreading in cross-stream direction could be attributed to the smaller velocity gradient between primary and secondary jet, which directly affects the entrainment from secondary flow. However, in the case of hydrogen injection the velocity gradient along the transverse direction is higher as the velocity of primary flow for same Mach number is approximately four-times that of ethylene.

The velocity profile along the downstream locations is another parameter which throws light on the behavior of jet evolution and mixing characteristics. In Fig. 7(b), normalized velocity profiles are presented; the normalization for both the cases is done by the fuel jet exit velocity of the respective fuels, details of which are provided in Table 1.

At $x = 83$ *mm* for all the cases the symmetric profile initially remains constant ($\pm 2 < y < \pm 4$), and upon reaching the recirculation region ($0 < y < \pm 2$) it reduces and then increases towards the core of jet to attain the maximum velocity. Worth noticing is the larger and wider low velocity region for the Straight strut cases (SS) compared to the Tapered strut cases (TS). When comparing TS and SS cases, particularly at $x = 83$ *mm*, the flow accelerates just before it reaches the recirculation region, as observed for both the injection cases, but this acceleration is more pronounced for the ethylene cases. Furthermore, with the increasing jet diameter this acceleration of the flow is decreased outside the recirculation region on either side of jet, which is primarily due to the reduction in the taper angle for the higher jet diameter as the flow turns through the expansion fan, the strength of which decreases with the taper angle. At other locations further downstream of the jet injection $x = 83$ *mm*, for H_2 injection the velocity profile tends to become more flat due to the larger entrainment from the surrounding secondary flow compared to the C_2H_4 and this can be noticed for both the strut geometries.

3.3 Total pressure decay

In any study involving supersonic mixing or combustion, two parameters widely accepted for the characterization of any injection technique are total pressure and temperature decay, suggested by Refs. [7, 15, 30]. However due to freestream temperature of primary and secondary flow being approximately same, total temperature decay cannot be a good indicator of mixing characteristics. Total temperature decay is primarily a good parameter for studies involving a significant

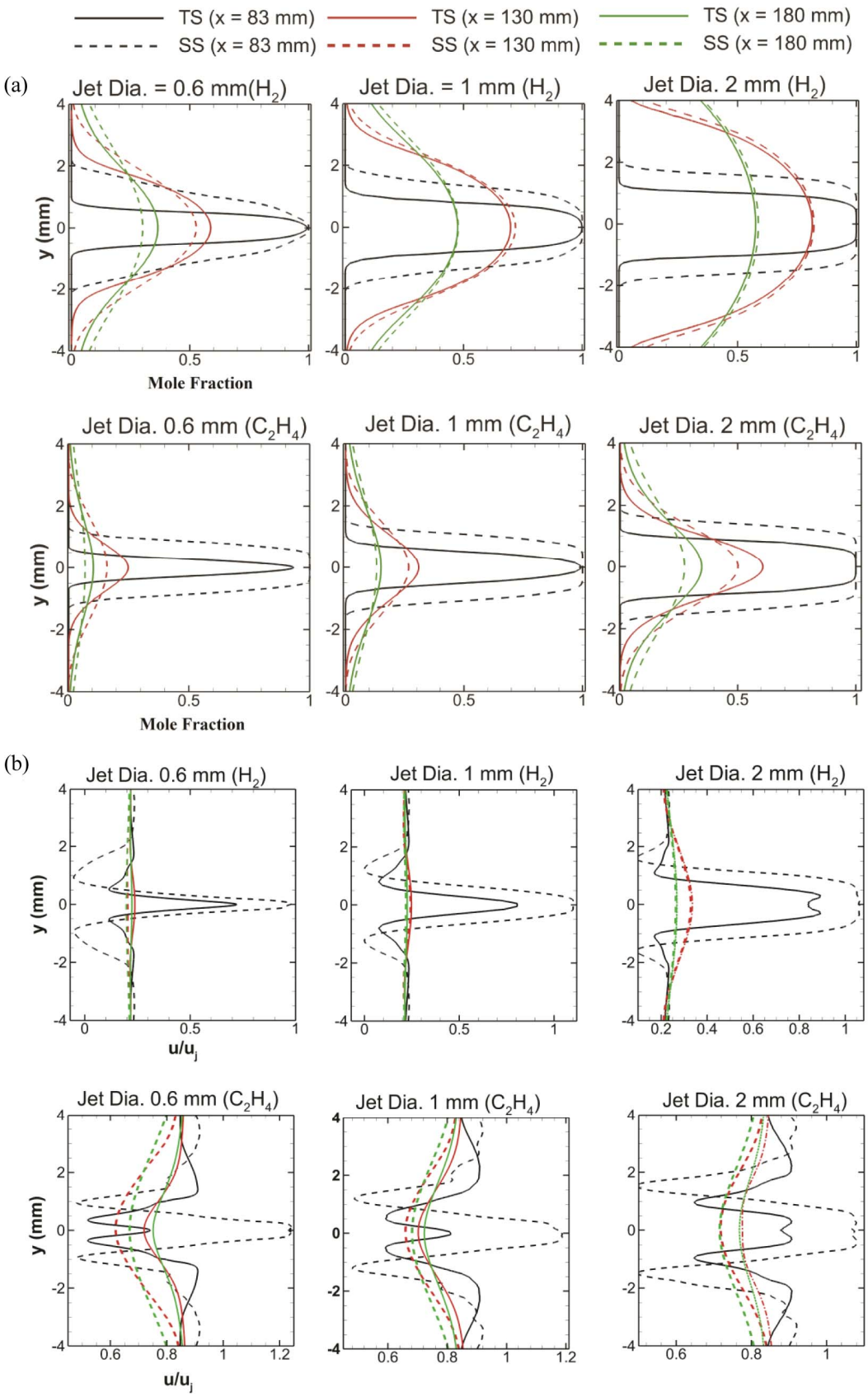

Fig. 7. (a) Mole fraction; (b) velocity profile at different locations.

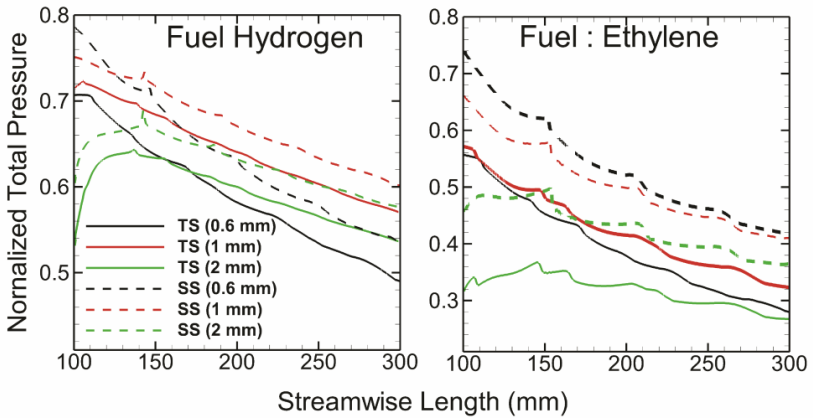

Fig. 8. Total pressure decay for both H_2 and C_2H_4 for varying jet diameter for both the strut.

temperature difference. Hence, in the present case only total pressure decay along the jet centerline is discussed.

Total pressure decay (TPD) is a good indication of the spreading rate and mixing characteristics. The increased decay in total pressure distribution is indication of higher spreading rate and enhanced mixing rate. Fig. 8 presents normalized total pressure along the jet centerline where stagnation pressure is normalized as $(P_{o,j} - P_o)/P_{o,j}$.

The decay is higher for the 0.6 mm case with H_2 injection; however, worth noticing is the difference between TS-0.6 and SS-0.6. This difference suggests that the SS-0.6 case has slightly higher spreading rate, which can be confirmed from the Fig. 6. As observed in Fig. 6, the growth rate of the jet is slightly more compared to TS-0.6. This is because a stronger reattachment shock is created for the SS-0.6 mm case, which can be verified from Fig. 6, compared to the other two, which is consistent with the observation of Ref. [13].

This observation is consistent with the observations of velocity and mole fraction profiles. Overall, hydrogen appears to have a desirable mixing and spreading rate for supersonic combustion. Also, it can be inferred that hydrogen would require shorter length compared to ethylene for better mixing. The increased entrainment of secondary flow in the primary flow is higher for hydrogen for all jet diameters, while the same appears to be much less for the ethylene case. Note that the present investigation reveals that the overall SS configuration seems to perform better than the TS cases for all the jet diameters, as it offers a stronger recirculation region near the jet exit.

Keeping the above-mentioned discussion in mind, the most promising configuration from the present study appears to be SS-0.6 mm cases. From the total pressure decay observation, it is found that for 0.6 mm H_2 case, SS configuration has around 11 % more total pressure decay than the TS-0.6 mm configuration, which is evident from the species molar fraction distribution. Similarly, in case of C_2H_4 injection SS-0.6 mm offers 19 % more total pressure decay than the TS-0.6 mm case. For higher jet diameter the percentage change is almost negligible, especially in case of 2 mm injection. In general, SS configuration appears to be more promising; however, with increasing diameter the combustor length required to achieve near field mixing appears to be increased; while for higher jet diameter the SS configuration might require stronger shock to keep the combustor length optimum.

3.4 Mixing efficiency

Finally, mixing efficiency (η_m) for all geometrical variation and both fuel has been computed based on the relation coined at NASA Langley Research Center [31]. The two-part definition is given in Eqs. (17) and (18).

$$\eta_m = \frac{\int Y_f \rho u \, dA}{\int Y \rho u \, dA} \tag{17}$$

where

$$Y_f = \begin{cases} Y, & Y \le Y_s \\ Y_s\left(1-Y\right)/\left(1-Y_s\right), & Y > Y_s \end{cases}. \tag{18}$$

Mixing efficiency is that fraction of least available reactant that can react as the mixture is brought to chemical equilibrium. The value of η_m varies from 0 to 1, where $\eta_m = 0$ represents perfectly segregated jet, whereas $\eta_m = 1$ is the indication of perfectly mixed system.

Fig. 9 presents the mixing efficiency for both H_2 and C_2H_4 for all jet diameters corresponding to both geometries. Similar to earlier observations, here once again, SS-0.6 mm for both ethylene and hydrogen exhibits excellent mixing characteristics. For the 0.6 mm case, SS requires lesser combustor length compared to TS case. SS-0.6 (H_2) achieves 100 % mixing efficiency at about 225 mm, which is also the same for SS-0.6 (C_2H_4); however, TS-0.6 (H_2) achieves similar efficiency at around 275 mm, whereas TS-0.6 (C_2H_4) requires 300 mm to attain similar mixing efficiency. For higher diameters similar observation is noticed, in case of hydrogen injection the mixing efficiency for 1 mm case is almost 60 %, whereas it decreases to 40 % for the 2 mm case. This observation again

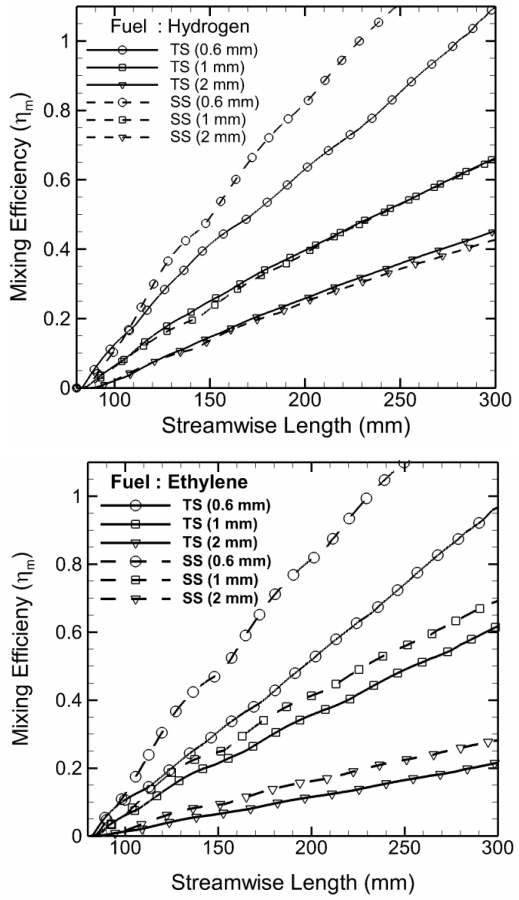

Fig. 9. Mixing efficiency along the jet centerline.

suggests the need for a longer combustor to achieve near field mixing or stronger shock generation through ramp for 1 and 2 mm diameter.

Finally, a quantitative comparison for all cases is presented in Table 3. For comparing the performance of different combination mixing efficiency, combustor length and Total pressure decay (TPD) are presented. The TPD here is the difference between jet exit and domain outlet, calculated from Fig. 8. From Table 3 it is evident that overall the SS configuration performs better than the TS configuration for both the fuels. However, the increase of jet diameter can be seen from the combustor length required for complete mixing.

The total pressure decay from Table 3 points out that for the entire cases hydrogen injection offers better spreading rate compared to the ethylene, as for all cases the TPD is always higher as opposed to the ethylene injection. The increased decay points toward the enhanced entrainment of primary air in the jet region, which is consistent with the observation of Fig. 7(b).

4. Conclusions

Numerical simulation of supersonic planar jet has been performed for two configurations with hydrogen and ethylene as fuel. A validation and grid independence study is performed and the acceptable accuracy in the numerical realization has given confidence for further detailed study. Also, the effects of strut geometry for different planar jet with two fuels are performed. The observation of the overall exercise is provided categorically:

(1) Wall pressure and radial profile of mole fractions are found to be satisfactory. The difference in reattachment region due to lip thickness appears to play a crucial role in the mixing phenomenon.

(2) The mole fraction profiles for both fuels suggest hydrogen to be the better candidate for the given strut geometry. SS configuration with hydrogen is found to be more promising. Better spreading for fuel jet is observed for SS configuration, but for higher jet diameter the performance deteriorates, especially in the case of 2 mm. In general, it can be inferred that mixing effectiveness decreases with increasing jet diameter for a given configuration.

(3) Total pressure decay is higher for the hydrogen case, suggesting better mixing efficiency and spreading rate, especially for the SS cases.

(4) Mixing efficiency results are consistent with the total pressure decay observations.

(5) Taper angle and extent of recirculation region had a direct effect on the near-field mixing.

Table 3. Quantitative comparison of various parameters.

Fuel	Dia. (mm)	η_m (%)	Length (mm)	TPD
H_2	**TS**			
	0.6	100	275	0.27
	1	60	300	0.21
	2	40	300	0.02
	SS			
	0.6	100	225	0.30
	1	60	300	0.25
	2	40	300	0.06
C_2H_4	**TS**			
	0.6	100	225	0.21
	1	60	300	0.12
	2	20	300	0.01
	SS			
	0.6	97.5	300	0.25
	1	64	290	0.15
	2	25	300	0.02

Acknowledgment

Financial support for this research is provided through IITK-Space Technology Cell (STC). Also, the authors would like to acknowledge the High Performance Computing (HPC) Facility at IIT Kanpur (www.iitk.ac.in/cc).

Nomenclature

ρ	: Density
T	: Temperature
P	: Pressure
u_i, u_j	: Velocity
δ_{ij}	: Kronecker delta
μ_t	: Eddy viscosity
ω	: Specific dissipation rate
k	: Turbulent kinetic energy
γ	: Specific heat ratio
M	: Mach number
η_m	: Mixing efficiency
χ	: Species mole fraction
Y_f	: Species mass fraction
Y_s	: Stoichiometric mass fraction (0.0292 for H_2 – air, 0.068 for C_2H_4 – air)

Subscripts

o	: Stagnation condition
∞	: Freestream condition
j	: Jet exit condition

References

[1] M. J. Barber, J. A. Schetz and L. A. Roe, Normal, sonic helium injection through a wedge-shaped orifice into supersonic flow, *J. of Propulsion and Power*, 13 (2) (1997) 257-263.

[2] R. A. Baurle, R. P. Fuller, J. A. White, T. H. Chen, M. R. Gruber and A. S. Nejad, An investigation of advanced fuel injection schemes for scramjet combustion, *AIAA Paper*, 98-0937, Jan. (1998).

[3] J. Belanger and H. G. Hornung, Transverse jet mixing and combustion experiments in hypervelocity flows, *J. of Propulsion and Power*, 12 (1) (1996) 186-192.

[4] D. W. Bogdanoff, Compressibility effects in turbulent shear layer, *AIAA J.*, 21 (6) (1983) 926-927.

[5] D. W. Bogdanoff, Advanced injection and mixing techniques for scramjet combustion, *J. of Propulsion and Power*, 10 (2) (1994) 183-190.

[6] G. L. Brown and A. Roshko, On density effects and large scale structures in turbulent mixing layers, *J. of Fluid Mechanics*, 64 (4) (1974) 775-816.

[7] B. V. N. Charyulu, J. Kurian, P. Venugopalan and V. Sriramulu, Experimental study on mixing enhancement in two dimensional supersonic flow, *Experiments in Fluids*, 24 (4) (1998) 340-346.

[8] S. L. N. Desikan and J. Kurian, Strut-based gaseous injection into a supersonic stream, *J. of Propulsion and Power*, 22 (2) (2006) 474-477.

[9] O. Dessornes and C. Jourdren, *Mixing enhancement techniques in a scramjet*, Office National D Etudes Et de Recherches Aerospatiales Onera-publications-TP (1998).

[10] P. E. Dimotakis, *Turbulent free shear layer mixing and combustion, High Speed Flight Propulsion Systems*, S. N. B. Murthy and E. T. Curran (Ed.), Progress in Astronautics and Aeronautics, AIAA, Washington, DC, 137 (1991) 265-340.

[11] J. M. Donohue, H. Haj-Hariri and J. C. McDaniel, Vorticity generation mechanisms in parallel injection schemes for supersonic mixing, *AIAA Paper*, 3286 (1992).

[12] F. Genin and S. Menon, Simulation of turbulent mixing behind a strut injector in supersonic flow, *AIAA J.*, 48 (2010) 526-539.

[13] P. Gerlinger and D. Bruggemann, Numerical investigation of hydrogen strut injections into supersonic airflows, *J. of Propulsion and Power*, 16 (1) (2000) 22-28.

[14] T. Sunami, M. Nishioka, A. Murakami and K. Kudou, Alternating- wedge strut injection for supersonic mixing and combustion, *14th International Symposium on Air Breathing Engine*, Italy National Organizing Committee, ISABE 99-7156 (1999).

[15] E. Gutmark, K. C. Schadow and K. J. Wilson, Effect of convective Mach number on mixing of coaxial circular and rectangular jets, *Physics of Fluids A: Fluid Dynamics*, 3 (1) (1991) 29-36.

[16] J. M. Seiner, S. M. Dash and D. C. Kenzakowski, Historical survey on enhanced mixing in scramjet engines, *J. of Propulsion and Power*, 17 (6) (2001) 1273-1286.

[17] K. Y. Hsu, C. D. Carter, M. R. Gruber, T. Barhorst and S. Smith, Experimental study of cavity-strut combustion in supersonic flow, *J. of Propulsion and Power*, 26 (6) (2010) 1237-1246.

[18] S. H. Kim et al., Large eddy simulation based studies of reacting and non-reacting transverse jets in supersonic cross-flow, *50th AIAA Aerospace Sciences Meeting Including the New Horizons Forum and Aerospace Exposition* (2012).

[19] C. R. Hyde, B. R. Smith, J. A. Schetz and D. A. Walker, Turbulence measurements for heated gas slot injection in supersonic flow, *AIAA J.*, 28 (9) (1990) 1605-1614.

[20] J. Lee, Numerical study of mixing in supersonic combustion research and hypersonic applications, *J. of Propulsion and Power*, 10 (3) (1994) 297-304.

[21] G. Masuya, T. Komuro, A. Murakami, M. Murayama and K. Ohwaki, Ignition and combustion performance of scramjet combustors with fuel injection struts, *J. of Propulsion and Power*, 11 (2) (1995) 301-307.

[22] T. Sunami, N. W. Michael and M. Nishioka, Supersonic mixing and combustion control using streamwise vortices, *AIAA Paper* (1998) 3217.

[23] A. Hellsten, Some improvements in Menter's k-omega-SST turbulence model, *29th AIAA Fluid Dynamics Conference*, AIAA-98-2554, June (1998).

[24] F. R. Menter, Two-equation eddy-viscosity turbulence models for engineering applications, *AIAA J.*, 32 (1994) 1598-1605.

[25] F. Menter and T. Esch, Elements of industrial heat transfer prediction, *16th Brazilian Congress of Mechanical Engineering (COBEM)* Nov. (2001).

[26] A. Kurganov and E. Tadmor, New high-resolution central schemes for nonlinear conservation laws and convection - diffusion equations, *J. Comput. Phys.*, 160 (1) (2000) 241-282.

[27] A. Kurganov, S. Noelle and G. Petrova, Semidiscrete central-upwind schemes for hyperbolic conservation laws and hamilton - jacobi equations, *J. Comput. Phys.*, 160 (2000) 720-742.

[28] C. Greenshields, H. Weller, L. Gasparini and J. Reese, Implementation of semi-discrete, nonstaggered central schemes in a colocated, polyhedral, finite volume framework, for high speed viscous flows, *International J. for Numerical Methods in Fluids*, 63 (1) (2010) 1-21.

[29] D. Cecere, A. Ingenito, L. Romagnosi, C. Bruno and E. Giacomazzi, Shock/boundary layer/heat release interaction in the hyshot II scramjet combustor, *Proceeding of 46th AIAA/ASME/SAE/ASEE Joint Propulsion Conference*, AIAA paper (2010) 7066.

[30] T. G. Tillman, W. P. Patrick and R. W. Paterson, Enhanced mixing of supersonic jets, *J. of Propulsion and Power*, 7 (6) (1991) 1006-1014.

[31] R. C. Rogers, A study of the mixing of hydrogen injected normal to a supersonic airstream, NASA TN D-6114 (1971).

Rahul Kumar Soni is a Ph.D. student at Indian Institute of Technology Kanpur. His research interests include high speed flow, large eddy simulation, and supersonic mixing.

Ashoke De is an Associate Professor at Indian Institute of Technology Kanpur. His research interests include advanced turbulent combustion modelling, fluid-structure interaction, supersonic flows, combustion instabilities, Lattice Boltzmann modelling and turbulence modelling.